Magnetic Tensor Sensor and Way-finding Method based on Geomagnetic Field Effects with Applications for Visually Impaired Users

Kok-Meng Lee, *Fellow, IEEE/ASME*; Min Li; Chun-Yeon Lin, *Member, IEEE*

***Abstract*—This paper presents a method utilizing geomagnetic field effects commonly found in nature to help the visually impaired persons (VIPs) navigate safely and efficiently; both indoor and outdoor applications are considered. Magnetic information indicating special locations can be incorporated as waypoints on a map to provide a basis to help the user follow a map that amalgamates the waypoints into spatial information. Along with a magnetic tensor sensor (MTS), a navigation system for helping VIPs more effectively comprehend their surroundings is presented. With the waypoint-enhanced map and an improved dynamic time warping algorithm, this system estimates the user's locations from real-time measured magnetic data. Methods using image data to enhance waypoints at dangerous locations are discussed. The MTS-enhanced method can be integrated into existing personal mobile devices (with built-in sound, image, video and vibration alert capabilities) to take advantages of the rapidly developing internet, global positioning systems (GPS) and computing technologies to overcome several shortcomings of blind-assistive devices. A prototype MTS-enhanced system for indoor/outdoor navigation has been developed and demonstrated experimentally. Although the MTS and algorithm are presented in the context of way-finding for a VIP, the findings presented here provide a basis for a wide range of applications where geomagnetic field effects offer an advantage.**

***Index Terms*:— Visually impaired, Blind, Perception, Geographic information system, Wayfinding, Navigation**

I. Introduction

For people who lost the optical ability to interpret their surroundings, way-finding that requires the person to navigate indoor or outdoor to the destination is often a daunting task. Recent advances in personal mobile devices capable of computing, communication and control (3C), digital imaging, and global positioning, which are widely available at affordable cost, offer potentials to enhance the global perception of the user's surrounds. However, these technologies are generally ineffective for uses by blind people, particularly in close range navigation. Inspired by the ability of some biological organisms to detect geomagnetic (earth-magnetic) fields as an orientation cue during migration or homing, this paper explores the use of geomagnetic field effects to extend the capability of personal devices to help blind people overcome some problems encountered in daily way-finding.

This work was supported in part by the U. S. National Science Foundation EFRI-M3C 1137172, and National Basic Research Program of China (973 Program Grant No. 2013CB035803). *Corresponding author: Kok-Meng Lee, email: kokmeng.lee@me.gatech.edu.*

K.-M. Lee M. Li and C.-Y. Lin are with the George W. Woodruff School of Mech. Eng. at Georgia Inst. of Tech., Atlanta, GA 30332 USA. K.-M. Lee is also Distinguished Professor of the State Key Lab. of Dig. Manuf. Equip. and Tech. and Sch. of Mech. Sci and Eng. at Huazhong Univ. of Sci. and Tech., Wuhan, Hubei, 430074, P. R. China.

Traditionally, visually impaired persons (VIPs) without residual vision rely on white canes or guide dogs for close range navigation. White canes are most widely used because they are inexpensive, lightweight and small, and can reliably detect sufficiently large obstacles (such as steps and uneven surface) near ground/floor level, but the users require to continuously scan the small area ahead of them. While guide dogs are effective travel aids, they themselves are difficult to be taken care of by the VIP. Fully trained guide dogs are very expensive and useful only for five years. As a result, it was estimated [1] that only 1% of the two million VIPs have guide dogs.

Many technologies have been applied to way-finding; for example [2] where auditory feedback was proposed as a navigation aid for the visually impaired. Methods for indoor/outdoor navigation can be broadly divided into three categories based on existing human-made signals, pre-deployed infrastructures and nature-generated physical fields. The 1st category utilizes signals such as Wireless Fidelity (Wi-Fi), FM radio, television and phone signals [3, 4]. As these signals were originally developed for transferring voice and/or picture information, their accuracy is generally less than desired for positioning. The 2nd category relies on pre-deployed infrastructures that use technologies such as ultra-wideband, radio frequency identification (RFID), ultrasound and infrared [5~8] for navigation. The latter two, ultrasound and infrared sensors, provide proximity information but offers no physics-based information about the object, and thus require infrastructures with embedded data for location information. Pre-deployed infrastructures are costly and have limited area coverage. More recently, GPS are widely used for outdoor navigation. However, GPS cannot operate well in areas inaccessible to good-quality satellite signals, and their resolution (typically 10m) are inadequate to avoid dangers in way-finding applications. The 3rd category takes advantages of some nature-generated physical parameters or signals (such as thermal infrared, acceleration and optical field) for positioning [9~11]. These natural or passive signal-based technologies offer a low-cost solution.

Methods on obstacle avoidance can be classified into human-generated (active) and nature-generated (passive) signals [12] with advantages and limitations similar to the above mentioned 2nd and 3rd categories for navigation respectively. Active-signal methods, which requires an emitter/receiver pair to generate/detect signals (like ultrasonic and sonar) to determine the existence of the obstacles and their locations [1, 13, 14], are less sensitive to environmental influences but have limited range of operation. Passive-signal

This article has been accepted for publication in a future issue of this journal, but has not been fully edited. Content may change prior to final publication. Citation information: DOI 10.1109/TMECH.2016.2582850, IEEE/ASME Transactions on Mechatronics

methods (for example, the uses of thermal infrared or optical fields [14] [15] naturally emitted/reflected from the obstacles to estimate the obstacle information), in general, have a potential to offer a low-cost solution.

High-resolution vision systems and algorithms are now widely available at relatively low-cost. Video information can be internet-transferred using personal digital assistant (PDA) without relying on pre-deployed or dedicated infrastructures. The VIP can share images/videos captured by a wearable camera through internet, which permit a remote sighted guide to navigate the VIP in the immediate travel environment [16, 17]. More recently, rapid developing social networks (such as Twitter, Facebook and RSS), which act essentially as a "social sensor", can further enhance the global perception of the surrounding environments [18]. However, these technologies are generally ineffective for close range way-finding by a VIP.

Magnetic sensing technology, inheriting many advantages of magnetic fields (such as great penetration, fast response, and well-defined theory), has been applied to help VIPs, such as reaching ferrous objects [19] and transmitting images via retinal stimulation [20]. The observations of geomagnetic distortion or anomalies in the presence of magnetic objects have led some researchers to develop geomagnetic based methods to help the VIPs navigate; for example, guide walking direction [21, 22] with a magnetic compass and localization utilizing the magnetic flux density (MFD) [23]. However, several barriers must be overcome for effective use of geomagnetic fields for way-finding: 1) Sensor range for geomagnetic anomaly is limited; 2) non-magnetic objects cannot be detected; 3) accurate survey of magnetic fields in 3D space is difficult to obtain; and 4) efficient algorithms for mapping localization with survey data remain lacking.

To overcome the above mentioned shortcomings of the passive methods that derive information from signals in nature, this paper presents a method based on geomagnetic field anomalies around ferrous objects for indoor/outdoor navigation. This method can be integrated into the existing devices (such as a VIP white-cane) and/or embedded in a personal mobile device (generally built with sound, image, video and vibration alert capabilities) to take advantages of the rapidly developing internet, GPS and digital imaging technologies; for example, camera-based assistive label reading for blind persons [24]. When complemented with imaging processing and GPS, the method presented here will have significant potentials to enhance the navigation experience of a VIP in both indoor and outdoor environments. The remainder of this paper offers the following:

– A magnetic tensor sensor (MTS) is introduced to enhance closed-range way-finding. The MTS utilizes direction-dependent geomagnetic-field effects to detect magnetic anomalies due to the presence of magnetic objects or current-carrying equipment. Magnetic anomalies exist almost everywhere and can be commonly found in modern buildings. Unlike traditional sensors that rely on direct MFD measurements, the MTS simultaneously measures the magnetic tensor **G** and MFD to determine the closeness and motion status of the magnetic object.
– Methods to incorporate geomagnetic effects and optical information as waypoints to define special locations (like pole, stair, gate and corner along a corridor) on a map are discussed, which provides a basis to estimate locations from the real-time measurements relative to the map.
– A navigation algorithm based on improved dynamic-time-warping (DTW) of magnetic data is presented. This new method which requires only 1D magnetic map greatly simplifies data collection. As will be shown, this method does not need the whole magnetic map after collecting the samples, and thus reduces sample sizes and search area.
– A prototype navigation system (that includes a MTS and takes advantages of existing vision and GPS technologies) has been experimentally evaluated; both indoor and outdoor applications are considered. This article focuses on assisting VIPs who obtain no visual information by themselves. Thus, this sensing method is applicable to a VIP who has residual vision as well as a healthy people.

II. Geomagnetic-field Magnetic Tensor Sensor (MTS)

Fig. 1 illustrates the design concept of a MTS for guiding visually impaired person. When a magnetic object is in space, the earth- magnetic (or geomagnetic) field around it is "distorted" as illustrated in Fig. 1(a). This distorted field can be used to derive information in the immediate surroundings of the VIP. However, the geomagnetic anomaly is difficult to be evaluated using direct MFD measurements. Thereby, the magnetic tensor **G** is utilized to interpret the geomagnetic effects. In addition, magnetic sensors in digital format are chosen to minimize the noise effect. Fig. 1(b) shows a prototype MTS consisting of two orthogonal pairs of digital 3-axis magnetic field sensors (BMC050) mounted at $\pm w/2$ (where w=10mm) from the x and y axes of the sensor local coordinate system. Packaged in a small footprint, BMC050 [25] has a relatively large measurement range, high resolution, low output noise, and low energy consumption; see Table I.

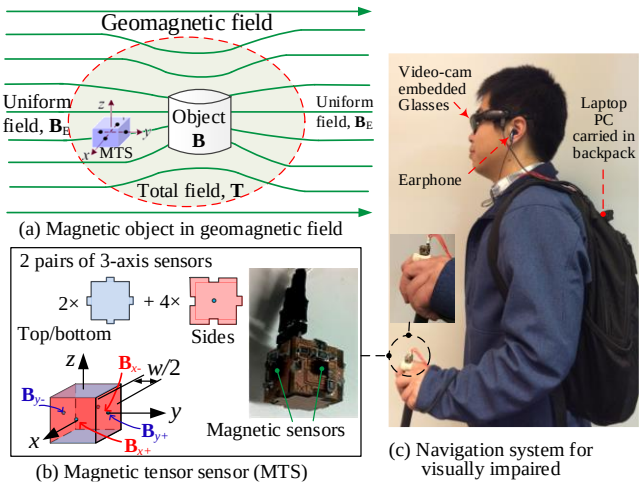

Fig. 1 Schematics illustrating MTS-based navigation system

In operation, the MTS communicates with a laptop PC through an inter-integrated circuit (I^2C) bus and an USB adaptor, where the MTS output signals are filtered using 1D median filter to remove noise. As will be shown, the MTS can

This article has been accepted for publication in a future issue of this journal, but has not been fully edited. Content may change prior to final publication. Citation information: DOI 10.1109/TMECH.2016.2582850, IEEE/ASME Transactions on Mechatronics

effectively supplement image-based information to improve the indoor/outdoor navigation of the visually impaired user. Carried in a backpack by the VIP as shown in Fig. 1(c), the MTS-measurements (with data from GPS and wearable camera) provide the user with surrounding information (by means of an earphone and/or stimulator).

Table I Sensor parameters

Three-axis magnetic sensor Model: BMC050		**Wearable digital video camera** Model: POV ACG-20	
Size (mm)	3×3×0.95h	Resolution (pixels)	1280×1024 (image)
Range(μT)	±1000		640×480 (video)
Resolution (μT)	0.3 (at 20Hz)	Frame rate	30 frames/s (FPS)
Output noise (μT)	0.3	Connection	Mini USB

A. Magnetic Sensor and Information for Way-finding

The total MFD at a point in space, denoted as **T** in (1), consists of $\mathbf{B_E}$ due to the geomagnetic field and **B** from the man-made magnetic objects as illustrated in Fig. 1(a):

$$\mathbf{T} = \mathbf{B_E} + \mathbf{B} + \mathbf{B_U} \tag{1}$$

In (1), $\mathbf{B_U}$ accounts for un-modeled magnetic field. Direct measurements of **B** are often challenging due to the relatively large earth magnetic field $\mathbf{B}_E$ (0.5G at mid-latitude) which must be eliminated from measurements. However, the geomagnetic field is relatively uniform, and its gradient is typically small as compared to that of the magnetic anomaly due to the man-made object; $|\nabla \mathbf{B_E}| \approx 0.02$ (nT/meter) and $\nabla \mathbf{T} \approx \nabla \mathbf{B}$ if $\mathbf{B_U}$ is negligible. Thus, a gradient-based sensor can more effectively detect the existence of a magnetic object.

The incremental difference in MFD can be written in the form of a 3×3 matrix (tensor) **G** in (2a), which is symmetric (2b) and traceless (2c):

$$\mathbf{G} = \frac{\partial \mathbf{B}}{\partial \mathbf{R}} = \begin{bmatrix} \partial_x B_x & \partial_y B_x & \partial_z B_x \\ \partial_x B_y & \partial_y B_y & \partial_z B_y \\ \partial_x B_z & \partial_y B_z & \partial_z B_z \end{bmatrix} \tag{2a}$$

$$\mathbf{G}^{\mathrm{T}} = \mathbf{G} \text{ and } \partial_x B_x + \partial_y B_y + \partial_z B_z = 0 \tag{2b, c}$$

where $\mathbf{B} = \begin{bmatrix} B_x & B_y & B_z \end{bmatrix}^{\mathrm{T}}$ and (∂_x, ∂_y, ∂_z) denote the partial derivatives with respect to $\mathbf{R} = [x \quad y \quad z]^{\mathrm{T}}$. Equation 2(c) can be directly derived from the divergence of **B** in free space $\nabla \bullet \mathbf{B} = 0$ which is one of the well-known Maxwell equations. For the way-finding and navigation applications, the sensor is in free space where (2c) is valid everywhere. Because of (2b) and (2c), only five elements of **G** require calculations:

$$\partial_x B_i = \frac{1}{w}\left(B_{i,x+} - B_{i,x-}\right) \text{and } \partial_y B_j = \frac{1}{w}\left(B_{j,y+} - B_{j,y-}\right) \tag{3a~e}$$

where $i = x, y, z$ and $j = y, z$; and $B_{i,x\pm}$ and $B_{i,y\pm}$ are the i^{th} MFD component from the sensor along the x and y axes respectively. The tensor **G** equals zero in a relatively uniform geomagnetic field. If the sensor is in its operating range, the MTS (while eliminating the influence of geomagnetic field) directly measures the field distortion, from which some object information can be derived from the magnetic properties.

1) Tensor-based parameter Q

Magnetic anomalies generated by objects are often difficult (if not impossible) to model because they are influenced by many factors (such as materials, shapes and its magnetic orientation relative to the geomagnetic field). Fortunately, humans do not rely on dimensionally accurate observations to make decisions as their non-contact feels are insensitive to small dimensional changes. Thus, two additional measurable parameters, Q and $d\mathbf{T}/dt$, are introduced in (4) and (5) where the dot over the variables represents their time derivatives:

$$Q = (1/2)\,\mathrm{tr}(\mathbf{G}^{\mathrm{T}}\mathbf{G}) \tag{4}$$

$$\left|\dot{\mathbf{T}}\right| = \sqrt{\dot{T}_x^2 + \dot{T}_y^2 + \dot{T}_z^2} \tag{5}$$

The parameter Q indicates the relative distance between the sensor and the magnetic object; and its value dramatically increases in magnitude as the sensor approaches the object. The parameters, **T**, Q and the absolute time-derivative $\left|\dot{\mathbf{T}}\right|$ in (1), (4) and (5) respectively, offer a means to determine the motion **Status** of the magnetic object relative to the sensor:

$$\mathbf{Status} = \begin{cases} 0 & \mathbf{T} \approx \mathbf{B}_E \text{ and } \left|\dot{\mathbf{T}}\right|, Q \to 0 \\ 1 & \text{Large changes in } \mathbf{T},\ \left|\dot{\mathbf{T}}\right| \text{ and } Q \\ 2 & \mathbf{T} \to \mathbf{T}_0,\ \left|\dot{\mathbf{T}}\right| \to 0 \text{ and } Q \to Q_0 \end{cases} \tag{6}$$

where $\mathbf{T}_0$ and Q_0 are constants. In (6), the **Status** 0, 1 or 2 indicate that there is no magnetic object, a moving magnetic object, or a magnetic object but stationary, respectively.

2) Illustrative simulation

The physical significance of the orientation-insensitive parameter Q is best illustrated with finite-element-analysis (FEA) numerically using commercial software, COMSOL. Many outdoor objects (such as fire hydrants, poles and traffic sign-posts) as well as indoor objects (like handrails) can be characterized as cylindrical steel objects which are thus chosen here for illustration and experimentally validated in Section III.B1.

As illustrated in Fig. 2(a), the steel object (where the XYZ coordinate system is assigned) is stationary in the uniform geomagnetic field (0.5G pointing in the Y direction). In order to comprehensively describe the geomagnetic field effects on the steel object, four different paths along which the MTS (at Z=0.8m) moves towards the object are simulated. The paths are denoted by φ = 0°, 30°, 60° and 90° measured clockwise from the X axis in Fig. 2(a). Simulation results are presented in Figs. 2(b, c, d) where MFD and Q are plotted as a function of the distance travelled, from which some observations are made:

- As Q is inversely proportional to a high-power of the distance between the MTS and the magnetic object [26], its values are graphed in a $\log_{10}$ scale for clarity. As the MTS moves near the object, $\log_{10} Q$ increases approximately linearly but is path-insensitive particularly for objects with a large aspect-ratio ($h/d \geq 5$). Unlike Q, the MFD and its gradient (magnitude/direction) are path-dependent.
- Q approaches zero monotonically as the MTS is far from the object for all cases whereas the measured MFD approaches a constant value equal to the geomagnetic field.

This article has been accepted for publication in a future issue of this journal, but has not been fully edited. Content may change prior to final publication. Citation information: DOI 10.1109/TMECH.2016.2582850, IEEE/ASME Transactions on Mechatronics

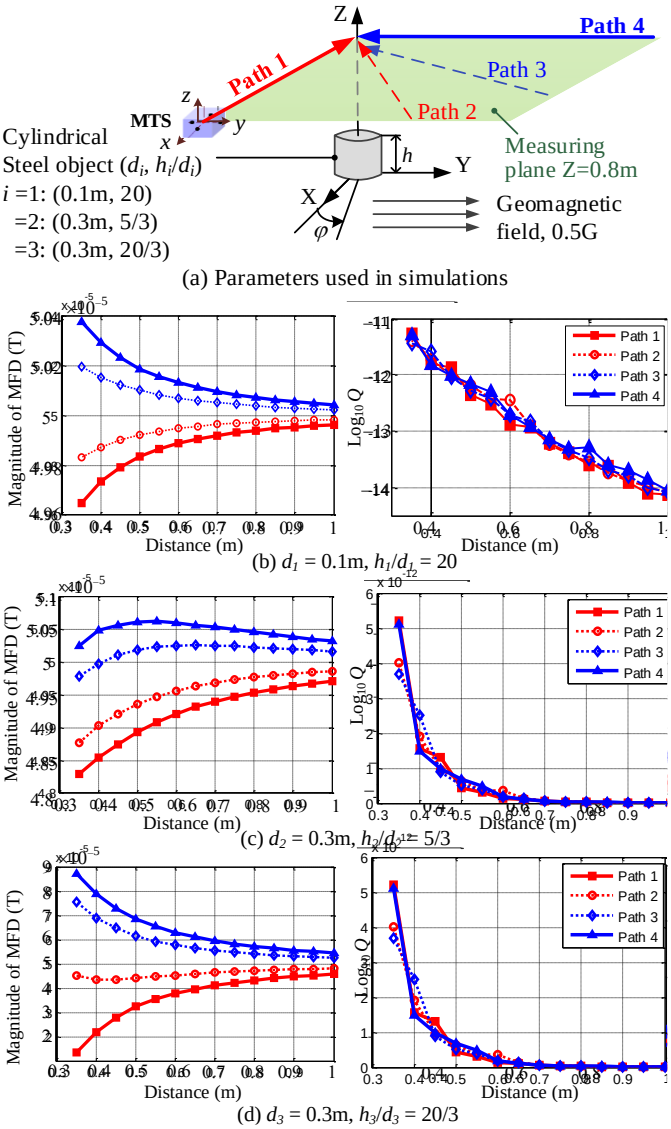

Fig. 2 Schematics and simulations showing effects on MFD and Q

B. *Dynamic Time Warping (DTW) for Map-Following*

The map-following method consists of a magnetic map, data collection and localization algorithm; the first two are closely related and inputs to the location algorithm analogous to a leader-follower approach. The leader prepares a 1D magnetic map along a route of interest to help the follower determine the location in real time by matching measured data with the prerecorded magnetic map. Since both the magnetic map and real-time sampled-data (that vary in time or speed under certain restrictions) are time-series with M and N elements respectively, the algorithm estimates the spatial location by evaluating similarities between the two temporal sequences to find an optimal alignment between them using a DTW method. The largest similarity implies that the magnetic samples most likely correspond to the location on the magnetic map. DTW is time-independent making it suitable for this application since travelers walk with different speeds and on varying paths.

Unlike the algorithms where numerical data are sent to machines for direct execution, the algorithm outputs qualitative information (for example, audio texts similar to that delivered to a GPS-guided car-driver) to human who generally has the knowledge and intelligence to make better decisions. Additionally, it must be computationally robust, and can be computed in real-time and embedded in a wearable device that is often limited in memory for computation. For robustness, an improved DTW method for processing multiple pairs of temporal sequences is formulated as a multi-dimensional problem to determine the 1D location along a route.

1) *Magnetic map and data collection*

Without relying on a two- or three-dimensional magnetic map which is often difficult to construct accurately, data collection along the 1D route is greatly simplified. In this method, magnetic data are pre-collected at a constant moving speed along the route of interest. The data themselves, however, do not contain location information and cannot be used for localization directly. To be effective, the magnetic data are coordinated on the floor map as *waypoints* to indicate "landmarks" (such as stair, gate and corner along a corridor) providing a reference to determine locations in real time. By mapping magnetic waypoints onto that of the floor map, spatial information is integrated to the magnetic map.

2) *Improved DTW algorithm for location estimation*

MTS simultaneously measures **T** (3 elements) and **G** (5 independent elements); each of the eight time-sequence pairs is associated with a cost. The element C_{mn} of the total cost matrix **C** for the m^{th} element of the map sequence ($\mathbf{x}_{\mathbf{B}m}$, $\mathbf{x}_{\mathbf{G}m}$) and n^{th} element of the sample sequence ($\mathbf{y}_{\mathbf{B}n}$, $\mathbf{y}_{\mathbf{G}n}$) is expressed as

$$C_{mn} = \mathbf{w}_{\mathbf{B}}^{\mathrm{T}}\mathbf{d}_{\mathbf{B}mn} + \mathbf{w}_{\mathbf{G}}^{\mathrm{T}}\mathbf{d}_{\mathbf{G}mn} \tag{7}$$

where $\mathbf{d}_{\mathbf{B}mn} = \left|\mathbf{y}_{\mathbf{B}n} - \mathbf{x}_{\mathbf{B}m}\right|$; $\mathbf{d}_{\mathbf{G}mn} = \left|\mathbf{y}_{\mathbf{G}n} - \mathbf{x}_{\mathbf{G}m}\right|$; and $\mathbf{w}_{\mathbf{B}}$ and $\mathbf{w}_{\mathbf{G}}$ contain the weight factors which are utilized to adjust the relative importance between the MFD **B** and its gradients for location estimation. In this paper, the weight factors are assigned to 1. The DTW method minimizes the total cost to determine an optimal alignment p for these two (map and sample) sequences, which intuitively runs along a "valley of low-cost" within the cost matrix **C**. Thus, the optimal alignment is also a warping path having a minimal total cost among all possible warping paths defined in (8a,b) where the subscript l indicates an element along the warping path with length L in **C**:

$$\mathrm{DTW}(\mathbf{x},\mathbf{y}) = \min\left\{c_p(\mathbf{x},\mathbf{y}) \,\middle|\, p \text{ is a } (M,N) \text{ alignment}\right\} \tag{8a}$$

$$\text{where } c_p(\mathbf{x},\mathbf{y}) = \sum_{l=1}^{L} C_{m_l n_l}. \tag{8b}$$

In (8b), $C_{m_l n_l}$ is the element chosen from each row of the cost matrix **C** such that the chosen L elements are connected forming a warping path. To avoid tedious computation (exponential in M and N) when finding the optimal path, an accumulated matrix **D** is generated; its element D_{nm} is the lowest accumulated cost or sum of the elements in **C** for an optimal alignment between the first n and m elements of the two sequences respectively:

$$D_{nm} = \mathrm{DTW}\left[\mathbf{x}(1:m), \mathbf{y}(1:n)\right] \tag{9}$$

This article has been accepted for publication in a future issue of this journal, but has not been fully edited. Content may change prior to final publication. Citation information: DOI 10.1109/TMECH.2016.2582850, IEEE/ASME Transactions on Mechatronics

The indices of the lowest cost path over **D** represent the optimally warped indices for the two time-series.

3) Illustrative example

Figs. 3 and 4 illustrate the leader-follower approach in the context of an indoor navigation.

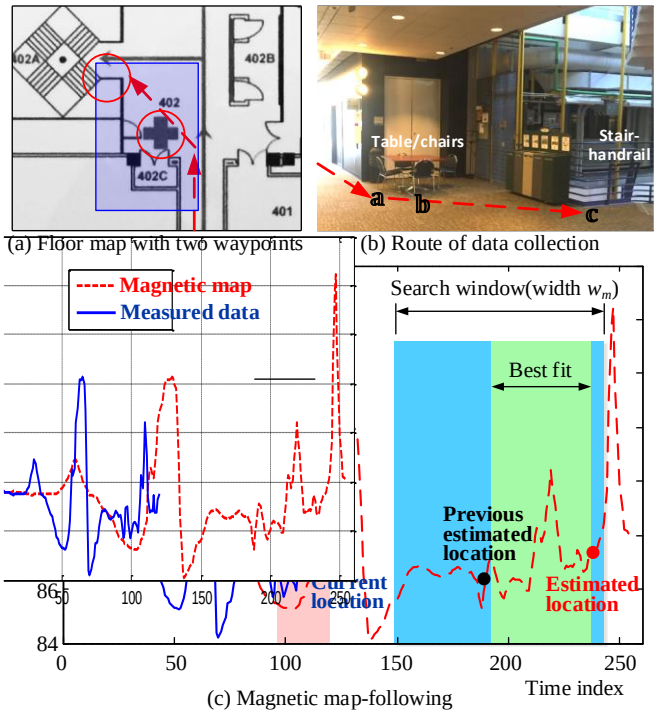

(a) Floor map with two waypoints (b) Route of data collection

(c) Magnetic map-following

Fig. 3 Magnetic map-following using improved subsequence DTW

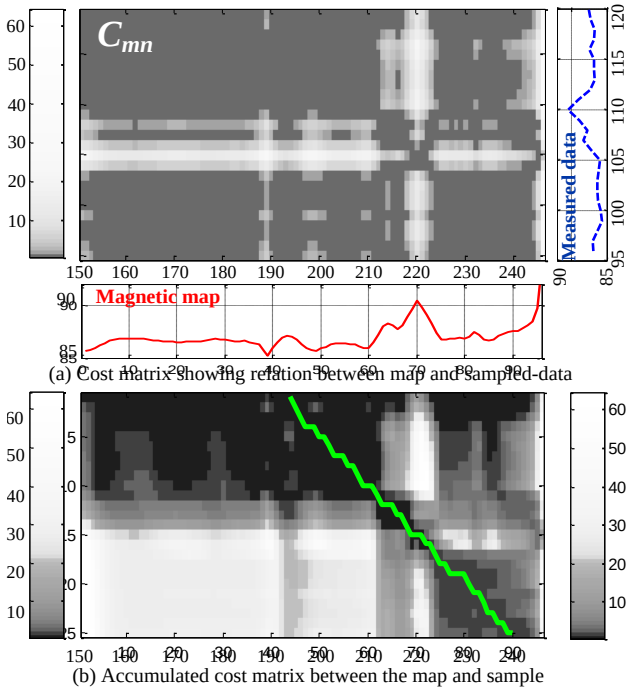

(a) Cost matrix showing relation between map and sampled-data

(b) Accumulated cost matrix between the map and sample

Fig. 4 Cost and accumulated matrixes and search windows

In Fig. 3(a), the red circles indicate the magnetic waypoints (table/chairs and handrails) as data are collected along the red dashed line in Fig. 3(a, b). The symbols **a** (chair), **b** (chair), and **c** (handrail) are detected waypoints appeared in Fig. 3(c) as local peaks on the map (red-dashed) and measured data (blue curve); only 1 of the 8 pairs is presented to avoid repetition. To estimate the current location (blue dot) near **c**, a sample-window (width w_d) determined by the data feature and a corresponding search window (width w_m) based on the previous location (black dot) are defined, which are shaded in pink and blue respectively. The costs are computed using the sequences in the sampled-data and search windows; the lowest cost indicates the best-fit window (shaded in green) where the calculated location (red dot) corresponds to current location blue dot) in the sampled-data window.

The location estimations using the improved DTW subsequence are detailed in Fig. 4(a) where the right and bottom plots of the cost matrix represent the data in sampled-data and search windows respectively. The optimal warping path (green line) for these two sequences is plotted on the accumulated matrix in Fig. 4(b). The path covers only the cells in the matrices that exhibit low costs. With the estimated optimal path, the spatial location can be estimated.

III. Applications and Experimental Results

The performance of the prototype MTS (Fig. 1b) and navigation system (Fig. 1c) has been experimentally evaluated involving both indoor and outdoor applications. The flowchart (Fig. 5) shows the relations among the magnetic map, magnetic/vision data collection and localization algorithms for the indoor (E1) and outdoor (E2) navigation examples. In E1, vision images are utilized to predict and identify an upcoming critical waypoint (such as a stair) or danger whereas in E2, vision images are introduced to extract and locate moving vehicles and zebra crossings. In both indoor and outdoor experiments, the MTS is attached to the VIP (at a height approximately 0.6m from the floor/ground); and the MTS coordinate system is defined such that its *y*-axis points to the moving direction. As will be shown, when coupled with information derived from images, magnetic information can significantly improve the safety of the blind user.

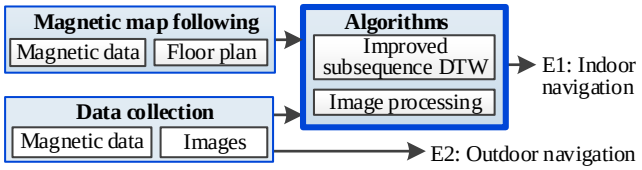

Fig. 5 Flowchart illustrating MTS-based applications

A. Magnetic Map Following for Indoor Navigation

Fig. 6 shows the emergency excavation route (Fig. 6a) of an office building and the magnetic map (Fig. 6b) for a VIP to follow, which provides the environment for the indoor navigation experiment to evaluate the prototype MTS and the location algorithm. The symbols ① to ⑧ indicating the waypoints (red numbers in Fig. 6a), which are specified landmarks and alert critical and dangerous locations along the path from Room 474 (red star) to the stair (red dot), are defined in Table II and Figs. 6(c, d).

1) Geomagnetic waypoints

Table II illustrates three different types of geomagnetic waypoints which are defined before data collection: The first

This article has been accepted for publication in a future issue of this journal, but has not been fully edited. Content may change prior to final publication. Citation information: DOI 10.1109/TMECH.2016.2582850, IEEE/ASME Transactions on Mechatronics

type is characterized by magnetic property in an object or a structure, which may be general steel or embedded components such as reinforced bars in a concrete pillar or column. The second type exists by virtue of its current-induced magnetic anomaly; the electrical closet ② where power lines, electrical equipment and network switches are housed is a good example. The third type is caused by the changes in sensor orientation relative to the uniform geomagnetic field without a magnetic anomaly (because geomagnetic field effects are directional); for example, the corner along the corridor ④ is a non-magnetic waypoint which helps locate the direction change. Unlike the 1st or 2nd type waypoint at which the specified location is defined, Waypoint ④ has little anomalies in the area but can be detected by the sensor after an actual geographical change in direction has taken place. For simplicity, only the MFD components along the route are shown here on the magnetic map in Fig. 6(b) which shows several significant MFD changes due to the magnetic waypoints marked in the pink-shaded window. The field changes at ④ and ⑥ are caused by the changes in sensor orientation relative to the uniform geomagnetic field, and that in ① to ③ and ⑤ are due to magnetic objects.

Table II Description of waypoints

①Pillar	②Electrical closet
③Pillar/Steel door frame	④Corner along the corridor
⑤Water dispenser	⑥End of corridor (elevator with first-aid box)
⑦Table and chairs	⑧Stair with steel handrails

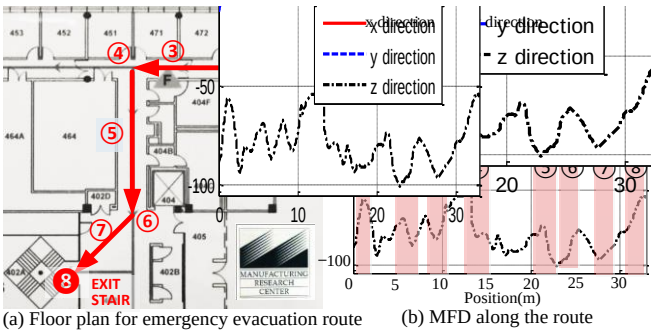

(a) Floor plan for emergency evacuation route (b) MFD along the route

(c) Objects along the route: pillars ①, ③, electrical closet ② and dispenser ⑤

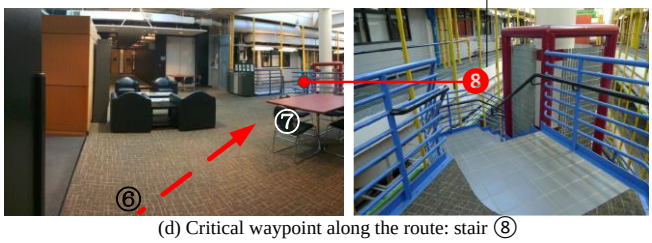

(d) Critical waypoint along the route: stair ⑧

Fig. 6 Schematics showing path/waypoints for indoor experiments

With the magnetic map, the localization algorithm described in Section II.B was utilized to estimate the actual location using measured **T** and **G**. The concept feasibility of the MTS-guided indoor navigation is evaluated by computing the errors of the estimated locations with respect to the actual locations. Based on four data sets collected along the route, the mean errors and their ranges at the eight waypoints are plotted in Fig. 7, the standard deviation of all experimental data is 81mm; and the position errors at stair-waypoint ⑧ are within ± 0.075m.

As shown in Fig. 7, the largest error occurs at ④ where the magnetic anomalies (or changes) are relatively small. The positive peak between Waypoints ④ and ⑤ is associated with the error in the corner ④ which is utilized to extract specified spatial/orientation information. In this method, the sensing system with its DTW algorithm uses the most recently collected data to estimate the current location and anticipate the corner-waypoint. Since the four different trails were not on the exact same path and did not make the left-turn on the same location and walk with the same speed, the variations in the estimation results (after the left-turn has actually occurred) should be expected. In this specific example, this specific waypoint represents a left-turn along the specified path from a 1.65m-wide corridor to a 2.5m-wide corridor; in other words, the positive peak (0.15m error) is less than 6% of the 2.5m range within which the VIP may make the turn. These results demonstrate the robustness and efficiency of this method.

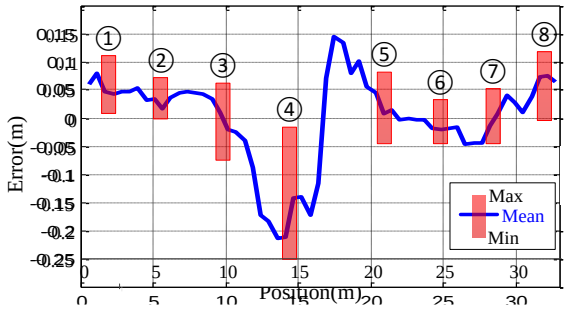

Fig. 7 Position errors

2) Image-enhanced waypoints for dangerous Location

Unlike the corner-waypoint ④ where some position errors around it are acceptably safe, position errors at stair-waypoint ⑧ could be dangerous for a VIP. To help guide the VIP stepping down the stairs safely, additional image-based data that offer predictive information are used to enhance the magnetic map by including the falling floor-edge and black-colored handrail as waypoint characteristics at ⑧. Without loss of generality, the widely known Hough-transform (HT) line-detection [27] and principal component analysis (PCA) color-classification vision algorithms [28] are used to characterize the falling floor-edge of the stairs (Fig. 8) and black-colored handrail (Fig. 9) in images captured by the wearable camera.

Fig. 8 illustrates the HT procedure (with ρ and θ as parameters in the straight-line equation) to define the path and detect the falling floor-edge. The procedure begins with searching in the two regions for the left and right side-lines ending at the floor-edge; $20° \le \theta \le 75°$ and $-75° \le \theta \le -20°$. Figs. 8(a, b) show the edge detection and HT results, where the

This article has been accepted for publication in a future issue of this journal, but has not been fully edited. Content may change prior to final publication. Citation information: DOI 10.1109/TMECH.2016.2582850, IEEE/ASME Transactions on Mechatronics

two peak values that characterize the (ρ, θ) parameters of the left and right side-lines occur at (774, 55.3°) and (–219, –61°). To locate the falling edge, a second HT is performed within the enclosed area bound by the two side-lines and a horizontal line as shown in Figs. 8(c, d, e). Computed using MATLAB, the time required to locate the falling edge from the original color images with resolution 1280×1024 and 640×480 were found to be 0.67s and 0.23s respectively.

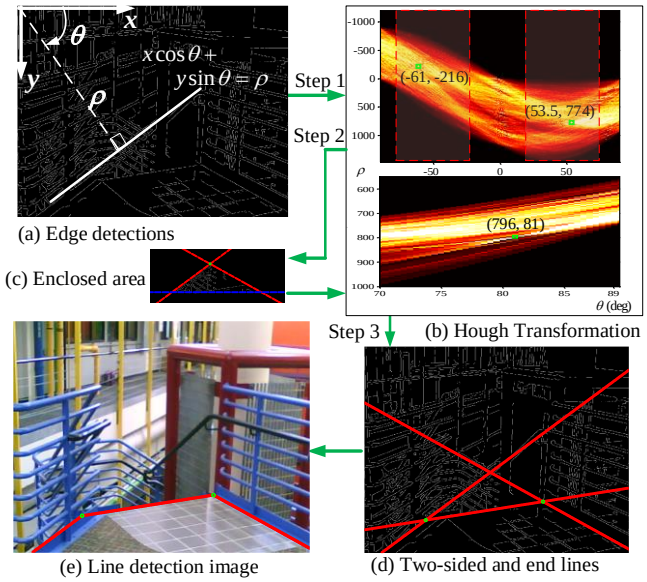

(a) Edge detections (c) Enclosed area (b) Hough Transformation (e) Line detection image (d) Two-sided and end lines

Fig. 8 Procedures of the algorithm applied at the stairs

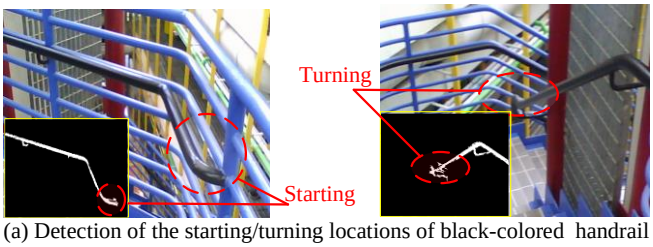

(a) Detection of the starting/turning locations of black-colored handrail

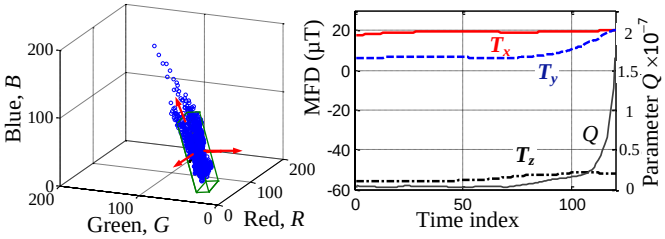

(b) Bounding box based on PCA (c) MFD and Q of the handrail

Fig. 9 Color-based object detection

Fig. 9 shows the procedure to detect the handrail using color segmentation to isolate the black-color followed by using MTS to detect the steel handrail. Five 20×20 pixels of the black-colored handrail are cropped from the RGB image for PCA-based color classification [28]. As shown in Fig. 9(b), a bounding box (with its boundary set at two standard deviations along the principal components axes from the mean RGB values) characterizes the black-color for filtering other colors. Pixels in the bounding box are extracted and followed by connected-component labelling with the size threshold value (=2% pixel number of the image) to filter out small fragments; the results are superimposed in Fig. 9(a). Fig. 9(c) illustrates the experimentally measured MFD components and calculated Q as the user's hand (with the MTS attached) moves in the direction that Q increases to reach the handrail by simply.

B. Outdoor navigation

The MTS and its wayfinding algorithm can be integrated into a VIP white cane (Fig. 10) and embedded in a personal mobile device to take advantages of the rapidly developing internet, GPS and digital imaging technologies to enhance the outdoor navigation experience of a VIP. To avoid repetition, experimental results of two practical applications are discussed here: The first analyzes the magnetic anomalies due to commonly seen objects along a typical outdoor walkway (Fig. 10), where the experimental results also serve as a basis for validating the observations in Fig. 2. The second illustrates some dangerous waypoints in the context of street-crossing.

B.1 Experimental illustration of the parameter Q

The observations in Fig. 2 were validated experimentally using the MTS described in Figs. 1(b, c) on three commonly seen outdoor objects (Objects 1, 2 and 3) and a vehicle; results are summarized in Figs. 10 and 11 respectively. In experiments for Fig. 10, the MTS moved along a path (geographically from east to west) towards each obstacle. Fig. 11 shows the MTS-measured data along the paths around the vehicle (2008 VW Passat). Similar to Fig. 2, Q approaches zero monotonically when the sensor is far from the object but each measured MFD approaches a constant corresponding to the path direction (relative to the geomagnetic field). Q increases drastically as the sensor moves near the object.

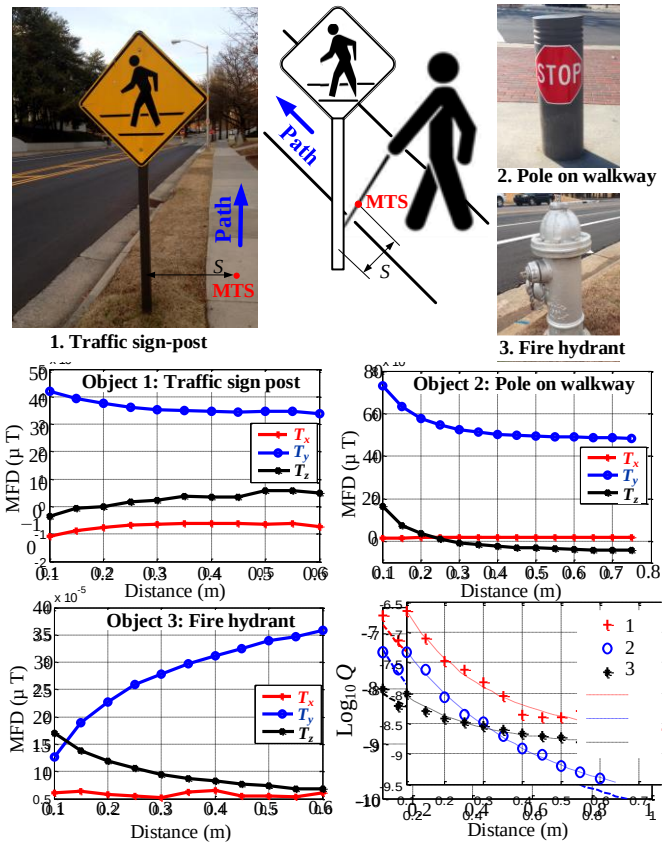

Fig. 10 Measured **B** and Q of stationary objects

This article has been accepted for publication in a future issue of this journal, but has not been fully edited. Content may change prior to final publication. Citation information: DOI 10.1109/TMECH.2016.2582850, IEEE/ASME Transactions on Mechatronics

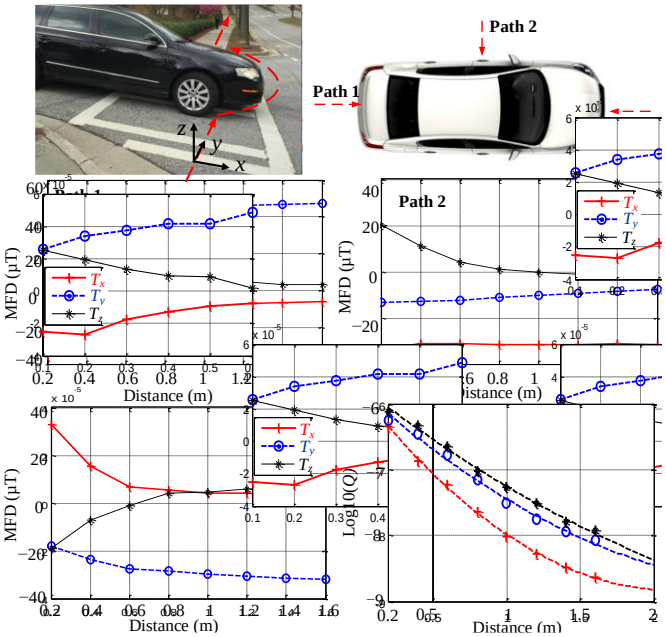

Fig. 11 Vehicle avoidance

B.2 Technology enhanced alidation

GPS are widely available in personal devices for outdoor navigation but their resolutions (<10m) are inadequate to help VIPs avoid obstacles along the path; for examples, signposts and moving vehicles are not on the map. While these obstacles can be easily avoided by healthy people, they cannot be seen by the VIPs. The MTS as an effective sensor for closed-range navigation is best illustrated with a practical example which begins at location ① with a screen-captured Google map showing the specific route photographed in Figs. 12(a, b). At ②, a commonly seen steel "stop" sign-pole (not on Google map) is on a pathway. The visually impaired user needs to avoid this obstacle before crossing the street at ③.

(a) Google Map

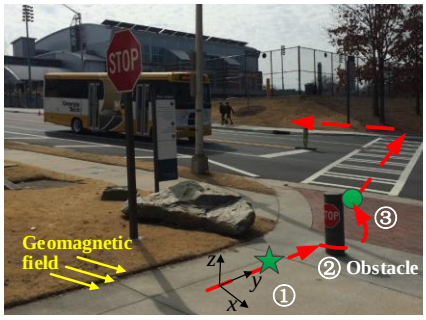

(b) Outdoor route

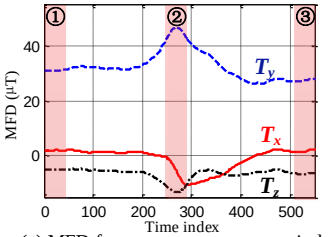

(c) MFD from green star to green circle

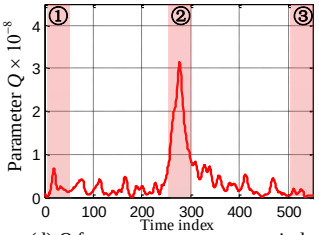

(d) *Q* from green star to green circle

Fig. 12 Experimental results illustrating outdoor obstacle avoidance

The flowchart (Fig. 13) summarizes the sensing, computing and decision processes of the outdoor navigation system. As shown in Fig. 13, the navigation system provides the (GPS, MTS and camera) information to the VIP to help derive decisions to overcome the following problems commonly encountered along the route:

– Avoids Stationary obstacles (Fig. 12c),
– Locate/follow a zebra-crossing (Fig. 14),
– Detect motion status of a vehicle (Figs. 15)

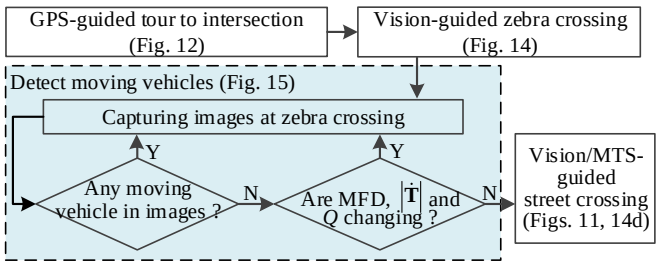

Fig. 13 Flow chart illustrating the process of outdoor navigation

(a) Google satellite map

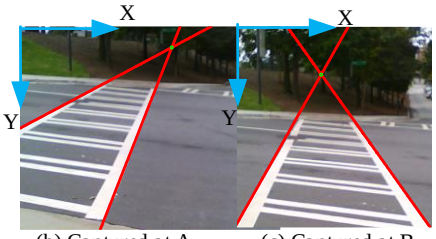

(b) Captured at A (c) Captured at B

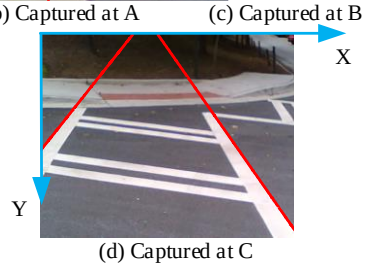

(d) Captured at C

Fig. 14 Zebra detection using vision image

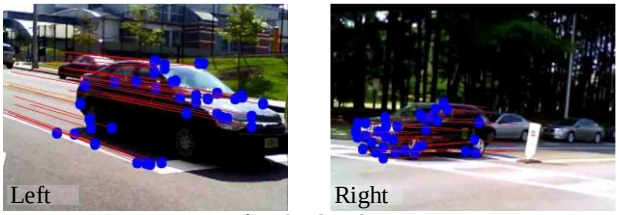

(a) Left and right side views

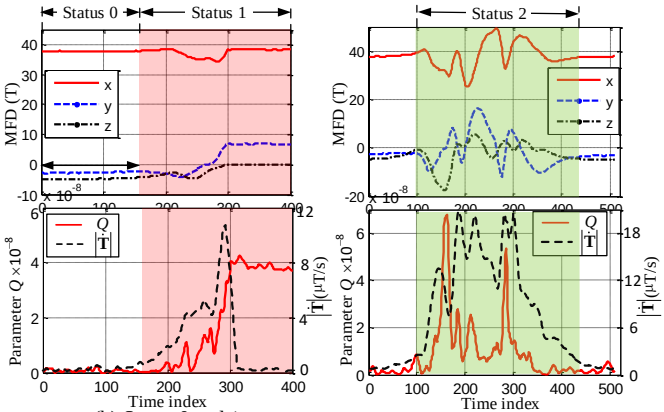

(b) Status 0 and 1 (c) Status 2

Fig. 15 Vehicles Detection

1) Avoidance of stationary obstacles

As photographed in Fig. 12(b), the VIP must avoid a steel "stop" sign-pole on the route. In this experiments, the sensor *y*-axis pointed in the moving direction (from east to west). The experimentally measured MFD components and calculated *Q* values along the path from ① (green star) to ③ (green circle) are plotted in Figs. 12(c, d). Because the steel-pole obstacle ② distorts the geomagnetic field, its presence is detected by the blind user carrying a MTS which calculates the *Q* values in real time. As shown in Fig. 12(d), the *Q* value increases dramatically as the people approach the obstacle signaling the user to go around to avoid the obstacle.

2) Locate/follow the zebra-crossing

Fig. 14(a) shows a GPS bird-eye view of the zebra-crossing that is not perpendicular to the street. To help the VIP walk within the bounds, the wearable camera captured images as the person walks. Typical images captured at positions A, B and C are shown in Figs. 14(b, c, d) respectively. The two high-contrast straight (red) lines in each position image are detected using the HT method to mark the outlines of the zebra-crossing. The procedures for the HT are similar to that discussed in Fig. 8 except both lines are searched in the region ($-75° \le \theta \le 75°$). The VIP's position relative to the zebra-crossing can be determined from their slopes: For the case in Fig. 14, the two lines have negative slopes at A indicating the zebra-crossing is still on the left; once within the bounds at B or C, the two detected lines have opposite signs; and if the two slopes were positive, the person would have passed the zebra-crossing. The simple slope computation provides the basis for the image-based wayfinding at the zebra-crossing.

3) Detect motion status of the vehicle

Before crossing the street at position B (Fig. 14a), the VIP must ensure that there are no moving vehicles from all sides of the street. An optical flow method which describes the pattern of apparent object motion between two consecutive images caused by the movement of objects is utilized to overcome the limited range of the MTS. In this paper, the iterative Lucas-Kanade method [29] with pyramids in OpenCV library is used for a sparse feature set. For local streets where vehicle speeds are no more than 40 mph, the optical flow method detects any moving vehicle within 15m of distance. Fig. 15(a) illustrates typical optical flow results of the two images captured at position B, where the blue points mark the features; and the red lines display the motion trajectories.

As the vehicle approaches the zebra-crossing, the MTS detects the geomagnetic field distorted by the vehicle when it moves into the sensing range (a circle of approximately 2m radius). The detected changes in the distorted MFD or the time-derivative of **T** (5) can be utilized to determine the motion status of the vehicle. Figs. 15(b) and 15(c) compare the experimentally measured MFD (T_x, T_y, T_z) components, calculated *Q* values and time-derivative of **T** between **Status** 1 and **Status** 2 respectively, where **Status** 0 indicates no vehicle initially in the sensing range. Fig. 15(b) shows the case of **Status** 1, where the vehicle slows down and stops. In Fig. 15(c), the vehicle passes by the VIP without stopping; the VIP needs to wait until the motion **Status** equals to 0 or 1.

IV. Conclusion

A navigation method utilizing geomagnetic field effects to guide the VIPs has been presented. Through this method, magnetic information (indicating special locations like stair, gate and corner along a corridor) can be incorporated as *waypoints* on a floor map, which provides a basis to help the VIP follow a 1D map that amalgamates magnetic waypoints into spatial information using the improved DTW method.

Along with a prototype MTS, a navigation system that combines the advantages of the geomagnetic field effects commonly found in nature and the rapidly developing (internet, GPS, digital video imaging, and computing) technologies has been developed, which enables the user more effectively comprehending their surroundings. As compared to other navigation methods, the proposed method is low-cost because it bases on nature-generated physical fields. Meanwhile, the magnetic fields have favorable properties (such as great penetration, fast response and insensitive to environments) which make this method robust and effective. When complemented with imaging processing and GPS, the disadvantages of the magnetic field-based sensors, which include limited sensing-range and disability to detect non-magnetic objects, can be cost-effectively overcome, and the method presented here will have significant potentials to detect and avoid obstacles for both indoor and outdoor navigation. Both numerical and experimental results show that the orientation-insensitive tensor-based parameter *Q* is a useful indicator to gauge the closeness of a magnetic object; and when simultaneously measuring the MFD and its time-rate, the MTS can be used to determine the motion status of the moving magnetic object (such as a vehicle) within a circular range of approximately 2m radius. As compared to GPS resolution of 10m, the MTS-enhanced navigation is capable of relatively accurate magmatic-map following (with a maximum mean position error of 0.21m and 0.08m standard deviation).

Results also show that when coupled with information derived from images, magnetic information can significantly enhance the navigation performance of a VIP, especially for areas with large magnetic anomalies and/or potentially dangerous waypoints. The effectiveness of the MTS-enhanced method has been experimentally validated and illustrated with several practical applications; indoor magmatic-map following, obstacle avoidance and street-crossing at locations with no traffic lights.

Acknowledgement

The initial discussions and comments on the research needs from the Advisory Board members of the NSF-EFRI-M3C-Research for the Visually Challenged, which have provided the motivation for the work reported here, are greatly appreciated.

References

[1] I. Ulrich, and J. Borenstein, "The GuideCane-Applying Mobile Robot Technologies to Assist the Visually Impaired," *IEEE Trans. on Systems,*

Man, and Cybernetics-Part A: Systems and Humans, vol. 31, no. 2, pp. 131-135, Mar. 2001.

[2] R. Liu and Y.-X. Wang, "Auditory Feedback and Sensory Substitution during Tele-operated Navigation," *IEEE/ASME Transactions on Mechatronics*, Vol. 17, No. 4, 2012, pp. 680-686.

[3] B. Li, Y. Wang, H. K. Lee, A. Dempster, and C. Rizos, "Method for Yielding a Database of Location Fingerprints in WLAN," *IEE Proceedings-Communications*, vol. 152, 2005, pp. 580-586.

[4] V. Moghtadaiee, A.G. Dempster, and Samsung Lim, "Indoor Localization Using FM Radio Signals: A Fingerprinting Approach," *Int. Conf. on Indoor Positioning and Indoor Navigation*, Sep. 21-23, 2011, pp. 1-7.

[5] C. Ye, S. Hong, and A. Tamjidi, "6-DOF Pose Estimation of a Robotic Navigation Aid by Tracking Visual and Geometric Features," *IEEE Trans. on Auto. Sci. & Eng.*, vol. 12, no. 4, pp. 1169-1180, Oct. 2015.

[6] S. Gezici, Z. Tian, G. Giannakis, H. Kobayashi, A. Molisch, H. Poor, and Z. Sahinoglu, "Localization via Ultra-wideband Radios: a Look at Positioning Aspects for Future Sensor Networks," *Signal Processing Magazine, IEEE*, vol. 22, pp. 70-84, 2005.

[7] N. B. Priyantha, A. Chakraborty, and H. Balakrishnan," The Cricket Location-support System," *6th Annual Int. Conf. on Mobile Computing and Networking*, Boston, Massachusetts, US, Aug. 2000, pp. 32-43.

[8] R. Want, A. Hopper, V. Falcao, and J. Gibbons," The Active Badge Location System," *ACM Trans. on Info. Syst*. vol.10, pp. 91-102, 1992.

[9] D. Hauschildt, and N. Kirchhof, "Improving Indoor Position Estimation by Combining Active TDOA Ultrasound and Passive Thermal Infrared Localization," *8th Workshop on Positioning Navigation and Communication*, Apr. 7-8, 2011, pp. 94-99.

[10] B. Zhou, Q. Li, Q. Mao, W. Tu, and X. Zhang, "Activity Sequence-Based Indoor Pedestrian Localization using Smartphones," *IEEE Trans. on Human-Machine Systems*, vol. 45, no. 5, pp. 562-574, Oct. 2015.

[11] S. Kaluwahandi, and Y. Tadokoro, "Portable Traveling Support System Using Image Processing for the Visually Impaired," *Int. Conf. on Imaging Processing*, 2001, vol.1, pp. 337-340.

[12] D. Dakopoulos, and N. N.G. Bourbakis, "Wearable Obstacle Avoidance Electronic Travel Aids for Blind: A Survey," *IEEE Trans. on Systems, Man, and Cybernetics- Part C: Application and Reviews*, vol. 40, no. 1, pp. 25-35, Jan. 2010.

[13] B. Ando, S. Baglio, V. Marletta, and A. Valastro, "A Haptic Solution to Assist Visually Impaired in Mobility Tasks," *IEEE Trans. on Human-Machine Systems*, vol. 45, no. 5, pp. 635-640, Oct. 2015.

[14] B. Ando, "A Smart Multisensor Approach to Assist Blind People in Specific Urban Navigation Tasks," *IEEE Trans. on Neural Systems And Rehabitation Engineering*, vol. 16, no. 6, pp. 592-594, Dec. 2008.

[15] N. Bourbakis, S. K. Makrogiannis, and D. Dakopoulos, "A System-Prototype Representing 3D Space via Alternative-Sensing for Visually Impaired Navigation," *IEEE Sensors Journal*, vol. 13, no. 7, pp. 2535-2547, Jul. 2013.

[16] V. Garaj, Z. Hunaiti, and W. Balachandran, "Using Remote Vision: The Effects of Video Image Frame Rate on Visual Object Recognition Performance," *IEEE Trans. on Systems, Man, and Cybernetics-Part A: Systems and Humans*, vol. 40, no. 4, pp. 698-707, Jul. 2010.

[17] Z. Hunaiti, V. Garaj, and W. Balachandran, "An Assessment of a Mobile Communication Link for a System to Navigate Visually Impaired People," *IEEE Trans. on Instrumentation and Measurement*, vol. 58, no. 9, pp. 3263-3268, Sep. 2009.

[18] J. Xiao, S. L. Joseph, X. Zhang, B. Li, X. Li, and J. Zhang, "An Assistive Framework for the Visually Impaired," *IEEE Trans. on Human-Machine Systems*, vol. 45, no. 5, pp. 635-640, Oct. 2015.

[19] K.-M. Lee and M. Li, "Magnetic Field Localization Method for Guiding Visually Impaired Applications," *IEEE/ASME Advanced Intelligent Mechatronics (AIM) 2013*. Wollongong, NSW, Jul. 9-12, 2013, pp. 542-547.

[20] K.-M. Lee, and C.-Y Lin, "Design Concept of a Novel EM-Array Magnetic Scanning System for Continuous Motion Control of Maximum MFD," *IEEE/ASME Advanced Intelligent Mechatronics (AIM) 2014*. Besacon, France, Jul. 8-11, 2014, pp. 1581-1586.

[21] M. Nakajima, and S. Harurama "Indoor Navigation System for Visually Impaired People Using Visible Light Communication and Compensated Geomagnetic Sensing," *1st IEEE Int. Conf. on Communications in China*, Aug. 15-17 2012, pp. 524-529.

[22] T. Gallagher, E. Wise, B. Li, A. G. Dempster, C. Rizos, and E. Ramsey-Stewart, "Indoor Positioning System Based on Sensor Fusion for The Blind and Visually Impaired," *Int. Conf. on Indoor Positioning and Indoor Navigation*, Nov.13-15 2012, pp.1-9.

[23] B. Gozick, K. P. Subbu, R. Dantu, and T. Maeshiro, "Magnetic Maps for Indoor Navigation," *IEEE Trans. on Instrumentation and Measurement*, vol. 60, no. 12, pp. 3883-3891, Dec. 2011.

[24] C. Yi, Y. Tian, J. Barnes, and A. Arditi, "Portable Camera-Based Assistive Text and Product Label Reading From Hand-Held Objects for Blind Persons," *IEEE/ASME Transactions on Mechatronics*, Vol. 19, No. 3, 2014, pp. 808-817.

[25] Bosch Sensortec, "BMC050 Electronic Compass", BMC050 datasheet, Oct. 2011.

[26] K.-M. Lee, and M. Li, "Magnetic Tensor Sensor for Gradient-based Localization of Ferrous Object in Geomagnetic Field," *IEEE Trans. on Magnetics*, Pub. Online Feb. 2016, DOI: 10.1109/TMAG.2016.2535307.

[27] Image Processing Toolbox, MATLAB 7.0.4 (R14SP2) 1994-2015 The MathWorks, Inc

[28] Lee, K.-M.; Li, Q.; Daley, W, "Effects of Classification Methods on Color-Based Feature Detection with Food Processing Applications," *IEEE Trans. on Auto. Sci. and Eng*. vol. 4, no. 1, Jan. 2007 pp: 40-51.

[29] J. Y. Bouguet, "Pyramidal Implementation of the Lucas-Kanade Feature Tracker Description of the Algorithm", Intel Corporation, Microprocessor Research Labs, OpenCV Documents, 1999.

Kok-Meng Lee (M'89–SM'02–F'05) received the B.S. degree from the State University of New York, Buffalo, NY, USA, in 1980, and the S.M. and Ph.D. degrees from the Massachusetts Institute of Technology, Cambridge, MA, USA, in 1982 and 1985, respectively. He is currently a Professor in the George W. Woodruff School of Mechanical Engineering, Georgia Institute of Technology, Atlanta, GA, USA. He was also honored as Pao Yu-Kong Chair Professor at Zhejiang University. He is also Distinguished Professor with the State Key Laboratory of Digital Manufacturing Equipment and Technology, Huazhong University of Science and Technology, Wuhan, China, under the National Recruitment Program of Global Experts.

His current research interests include system dynamics/control, robotics, automation, and mechatronics. He holds eight patents in machine vision, a three-degrees-of-freedom (DOF) spherical motor/encoder, and a live-bird handling system.

Dr. Lee is a Fellow of the ASME. He received the National Science Foundation (NSF) Presidential Young Investigator, Sigma Xi Junior Faculty Research, International Hall of Fame New Technology, and Kayamori Best Paper Awards.

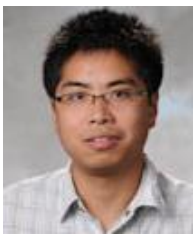

Min Li received the B.S. and M. S. degrees in Mechanical Engineering from the Huazhong University of Science and Technology, Wuhan, China in 2008 and 2011 respectively. Currently, he is Ph. D. Candidate in the George W. Woodruff School of Mechanical Engineering at Georgia Institute of Technology, Atlanta. His research interests include system dynamics/control, robotics, automation, and mechatronics.

Chun-Yeon Lin received the B.S. degree in mechanical engineering from National Central University, Taiwan in 2003, M. S. degree in electrical control engineering, National Chiao-Tung University, Hsinchu, Taiwan in 2005 and M. S. degree in mechanical engineering, Stanford University, Stanford, CA, in 2009. Currently, he is Ph.D. Candidate in the Woodruff School of Mechanical Engineering, Georgia Institute of Technology, Atlanta. His current research interests include mechatronics, machine vision, electromagnetic and intelligent system.